Ceramics International 43 (2017) 2246–2251

Contents lists available at ScienceDirect

Ceramics International

journal homepage: www.elsevier.com/locate/ceramint

Ultrahigh Q values and atmosphere-controlled sintering of $Li_{2(1+x)}Mg_3ZrO_6$ microwave dielectric ceramics

Jie Song, Jian Zhang, Ruzhong Zuo*

Institute of Electro Ceramics & Devices, School of Materials Science and Engineering, Hefei University of Technology, Hefei 230009, PR China

ARTICLE INFO

Keywords:
A. Sintering
B. X-ray methods
C. Dielectric properties

ABSTRACT

Ultrahigh-Q $Li_{2(1+x)}Mg_3ZrO_6$ microwave dielectric ceramics were successfully prepared by means of atmosphere-controlled sintering through simultaneously adopting double crucibles and sacrificial powder. This technique played an effective role in suppressing the lithium volatilization and further promoting the formation of the liquid phase, as evidenced by the X-ray diffraction, microstructural observation and the density measurement. Both dense and even microstructure, and the suppression of detrimental secondary phases contributed to low-loss microwave dielectric ceramics with $Q\times f$ values of 150,000–300,000 GHz. Particularly, desirable microwave dielectric properties of ε_r=12.8, $Q\times f$=307,319 GHz (@9.88 GHz), and τ_f=−35 ppm/°C were achieved in the x=0.06 sample as sintered at 1275 °C for 6 h.

1. Introduction

The tremendous development of wireless communications has stimulated the extension of utilizable frequency range to millimeter waves. Dielectrics are extremely desired to have an ultrahigh quality factor $Q\times f$ value (> 100,000 GHz) to reduce the risk of cross talk within a given frequency range, and a relatively low dielectric permittivity (ε_r < 20) to increase the speed of the signal propagation with minimum attenuation. Typical material candidates for this category of applications have included alumina, forsterite and willemite so far [1–7].

Recently, a novel ultra-low loss ceramic system of $Li_2Mg_3BO_6$ (B=Ti, Sn, Zr) with a rock-salt structure has been reported [8,9]. These ceramics sintered at 1280, 1360 and 1380 °C possessed excellent microwave dielectric properties of ε_r=15.2, 8.8 and 12.6, $Q\times f$=152,000, 123,000 and 86,000 GHz, and temperature coefficient of resonance frequency τ_f=−39, −32 and −36 ppm/°C, respectively [8]. However, the second phases Mg_2SnO_4 and ZrO_2 caused by lithium evaporation have deteriorated microwave dielectric properties of $Li_2Mg_3SnO_6$ and $Li_2Mg_3ZrO_6$ compounds, respectively. Actually, porous microstructure in these ceramics might also significantly degrade their $Q\times f$ values owing to the difficulty in sintering. Pure-phase $Li_2Mg_3BO_6$ ceramics were prepared by Wu et al. [10] through burying the sample pellets in sacrificial powder of the same composition. The atmosphere-protective sintering method could effectively overcome the lithium volatilization. As a result, the $Q\times f$ values of $Li_2Mg_3BO_6$ (B=Ti, Sn and Zr) ceramics were enhanced to 153,000, 145,000, and 113,000 GHz, respectively. Afterwards, $Li_2Mg_3TiO_6$ and $Li_2Mg_3SnO_6$ ceramics were further studied by a few research groups [11–13]. However, further studies of the $Li_2Mg_3ZrO_6$ ceramic were not found any more probably because of its lower $Q\times f$ values than the other two. In our previous work, excess lithium was added in $Li_2Mg_2(WO_4)_3$ and $Li_4Ti_5O_{12}$ ceramics to successfully eliminate the impurity phase, which was also induced by the volatilization of lithium [14,15]. In addition, excess lithium could also improve the sample density and reduce the sintering temperature for the purpose of achieving an improved microstructure as well as an enhanced $Q\times f$ value in lithium-containing materials [16,17].

In current work, a combination of excess lithium and powder-burying sintering technique was adopted to pursue a greatly enhanced $Q\times f$ value of $Li_2Mg_3ZrO_6$ ceramics. The phase structure, microstructure evolution and microwave dielectric properties of $Li_{2(1+x)}Mg_3ZrO_6$ (x=0–0.08) ceramics were systematically explored.

2. Experimental procedure

$Li_{2(1+x)}Mg_3ZrO_6$ (x=0–0.08) ceramic samples were prepared by a conventional mixed oxide method using high-purity raw powders: Li_2CO_3 (98.0%), MgO (98.5%), and ZrO_2 (99.0%) (Sinopharm Chemical Reagent Co. Ltd., Shanghai, China). Stoichiometric amounts of raw powders were weighed and milled with ZrO_2 balls in alcohol for 4 h. The wet mixtures were dried and then calcined at 1200 °C for 4 h. The calcined powders were ball-milled for 6 h again, then granulated with 5 wt% PVA as a binder after drying, and finally uniaxially pressed into cylinders with dimensions of 10 mm in diameter and 5–6 mm in height at a pressure of ~200 MPa. These samples were first heated at

* Corresponding author.
E-mail address: rzzuo@hotmail.com (R. Zuo).

http://dx.doi.org/10.1016/j.ceramint.2016.11.008
Received 20 October 2016; Received in revised form 1 November 2016; Accepted 2 November 2016
Available online 03 November 2016

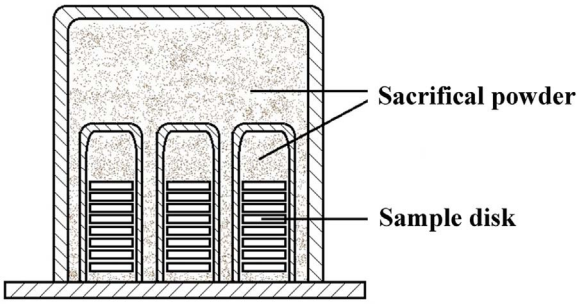

Fig. 1. Schematic plot of the sample placement for providing lithium-rich sintering atmosphere.

550 °C for 4 h to burn out the organic binder, and then sintered in air at temperatures from 1250 °C to 1325 °C for 6 h at a heating rate of 4 °C/min. In order to suppress the lithium evaporation, green pellets were placed into small crucibles, which were filled with the sacrificial powder and then covered with an alumina crucible lid on the top. Finally, a group of these small crucibles were covered by another larger alumina crucible, as schematically shown in Fig. 1. The above-mentioned double-crucible powder-burying sintering method was updated on the basis of previous work [10,18].

The bulk density of the sintered specimens was measured using the Archimedes method. The crystalline phases were identified by an X-ray diffractometer (XRD; D/Max2500V, Rigaku, Tokyo, Japan). Prior to the examination, the sintered pellets were crushed into powders with an agate mortar. The diffraction pattern was obtained over 10–90° at a step of 0.02°. The data were analyzed by the Rietveld refinement method using GSAS suite equipped with EXPGUI software [19,20]. The microstructure observation on the natural and fractured surfaces of the pellets was performed using a field-emission scanning electron microscope (FE-SEM; SU8020, JEOL, Tokyo, Japan) coupled with an energy dispersive spectroscope (EDS). Microwave dielectric properties of well-polished samples with an aspect ratio of 1.8–2.2 were evaluated with a network analyzer (Agilent, N5230C, Palo Alto, CA) and a temperature chamber (GDW-100, Saiweisi, Changzhou, China) by means of a Hakki-Coleman post resonator method [21]. The dielectric permittivity ε_r was measured using two parallel conducting plates and two coaxial electric probes as suggested by Courtney at the TE_{011} mode of resonance, which can be least perturbed by the surrounding field variation. For the measurement of the Q value, the sample was placed on a low-loss quartz support of 8 mm in diameter and 4 mm in height in the center of the silver-clad cylindrical shielded cavity (Resonant cavity, QWED, Warsaw, Poland). The loaded quality factor Q_L in transmission mode (S_{21} parameter) was determined from the full width of the resonance peak at the 3 dB level. The dielectric loss (tan δ) was calculated by using the software provided by the TE_{018}-shield cavity supplier, through which the Q values can be obtained in accordance with the equation Q=1/tan δ. All measurements were performed at room temperature in the frequency range of 8–12 GHz. The τ_f value of the samples was measured by noting the change in the resonant frequency over a temperature interval from 25 °C to 80 °C, as calculated by the following equation: $\tau_f=(f_2-f_1)/f_1(T_2-T_1)$, where f_1 and f_2 represent the resonant frequencies at T_1 and T_2, respectively.

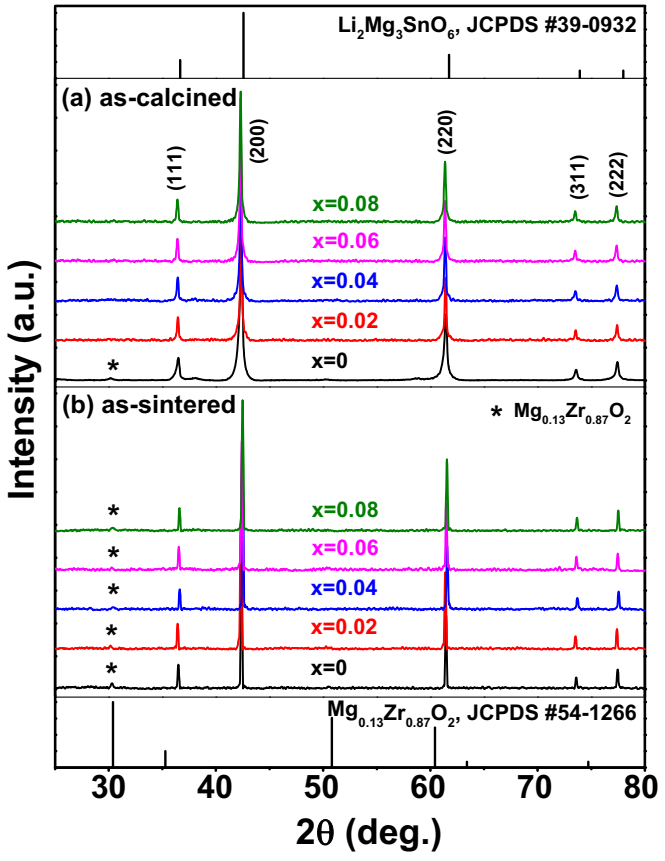

Fig. 2. XRD patterns of $Li_{2(1+x)}Mg_3ZrO_6$ samples (a) calcined at 1200 °C for 4 h and (b) sintered at 1275 °C for 6 h.

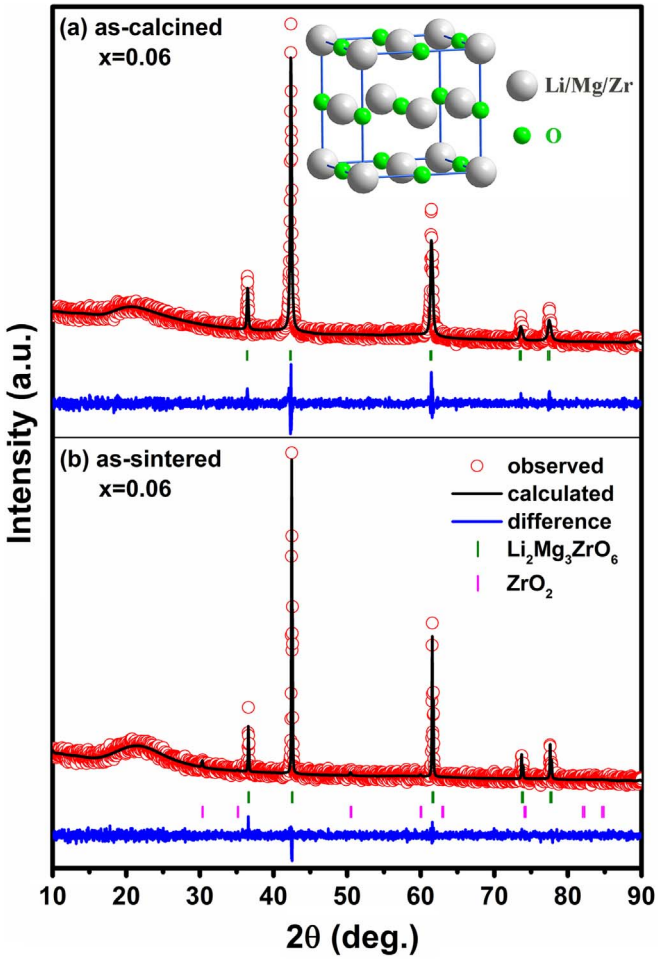

Fig. 3. Rietveld refinement plots of (a) as-calcined powder and (b) as-sintered sample at x=0.06. The inset schematically shows the $Li_2Mg_3ZrO_6$ crystal strucutre. (For interpretation of the references to color in this figure, the reader is referred to the web version of this article.)

Table 1
Ion occupancy in cubic $Li_2Mg_3ZrO_6$ crystal.

Atom	Position	x	y	z	Occupancy
Li	4a	0	0	0	0.33
Mg	4a	0	0	0	0.50
Zr	4a	0	0	0	0.17
O	4b	0.5	0.5	0.5	1

3. Results and discussion

The normalized XRD patterns of the as-calcined and as-sintered $Li_{2(1+x)}Mg_3ZrO_6$ powders are displayed in Fig. 2(a) and (b), respectively. Diffraction peaks of all calcined powder could be indexed to the standard pattern of cubic $Li_2Mg_3SnO_6$ (JCPDS #39-0932). It means that an isomorphic cubic $Li_2Mg_3ZrO_6$ with *Fm*-3*m* space group was formed in current work. Besides, it is noteworthy that a secondary phase $Mg_{0.13}Zr_{0.87}O_2$ (indexed to JCPDS #54-1268) also existed in the x=0 sample, but pure-phase $Li_2Mg_3ZrO_6$ could be obtained as $x > 0$, as shown in Fig. 2(a). This might result from the lithium volatilization in the matrix composition at a relatively high calcination temperature. However, excess lithium could compensate for lithium loss and then suppress the formation of the secondary phase in the calcined powder. Unfortunately, the secondary phase $Mg_{0.13}Zr_{0.87}O_2$ reappeared in the samples after sintering, as shown in Fig. 2(b). Moreover, the secondary phase surprisingly existed throughout all compositions with different lithium contents. These results seemed to be different from previous reports [8,10].

To confirm the phase composition and explore its evolution in more details, Rietveld refinement was carried out on the basis of the fine XRD data. TiN (ICSD #152807) and ZrO_2 (ICSD #92095) were chosen as the initial models for the matrix and secondary phase, respectively. Considering that some samples consisted of two phases as discussed above, a mixture model was employed for the structure refinement of these samples. TiN has the most similar structure to $Li_2Mg_3ZrO_6$ but the detailed ion occupancy should be revised before refinement. It could be clearly seen from the schematic of $Li_2Mg_3ZrO_6$ crystal in the inset of Fig. 3(a), that only two kinds of Wyckoff sites *4a* and *4b* exist in cubic $Li_2Mg_3ZrO_6$ with *Fm*-3*m* space group, and that there are two thirds of the $Li_2Mg_3ZrO_6$ molecule in a unit cell. All cations (Li^+, Mg^{2+}, Zr^{4+}), which coordinate with oxygen anions in a mode of octahedral structure [10], occupy the *4a* position, and oxygen anions occupy the *4b* position, as listed in Table 1. The as-calcined and sintered x=0.06 samples were chosen as representatives and their refinement plots are also shown in Fig. 3. The refined results from the calcined x=0.06 sample revealed the detailed structure information of single-phase $Li_2Mg_3ZrO_6$, such as the lattice parameters a=b=c=4.277(4) Å and α=β=γ=90°, and unit cell volume V=78.2(2) Å^3, which agreed well with the previous reports [8,10]. The refined structural parameters, reliability factors and goodness-of-fit indicator of as-sintered samples are summarized in Table 2. The observed and calculated diffraction profiles were found to keep a good agreement, as confirmed by relatively low amplitudes of the difference lines (blue lines in Fig. 3). The refinement reliable factors of R_{wp}, R_p, and χ^2 were found to be in the range of 7–10%, 5–8%, and 1.3–1.8, respectively, indicating that the structural model should be valid. It can also be found that the unit cell volume of the matrix $Li_2Mg_3ZrO_6$ in the x=0.06 sample decreased after sintering, primarily due to the lithium loss at high sintering temperatures. Lithium volatilization might be uneven in the ceramic sample and tended to cause a distortion of the unit cell. Overmuch lithium volatilization in the local area might lead to the instability of the unit cell, such that the secondary phase was always observed, as shown in Fig. 3(b). With increasing x, both the unit cell volume (V_1 and V_2) of $Li_2Mg_3ZrO_6$ and ZrO_2, and the weight percent (~1.5%) of the secondary phase showed a slight fluctuation, as shown in Table 2.

Fig. 4 indicates the microstructure of $Li_{2(1+x)}Mg_3ZrO_6$ ceramics sintered at 1275 °C. It seems that all the ceramics looked dense. There were two kinds of phases, such as the matrix grain and the impurity phase at the grain boundary, as shown in Fig. 4(a, c, e, g, and i). The initial spotty distribution of the impurity phase at x=0 gradually evolved into a continuous distribution at x=0.06. Overmany impurity phases then accumulated at the triangle grain boundary as x is beyond 0.06. The grain-boundary phase could be considered to be from liquid phases at high sintering temperatures. The liquid phase might result from the melting of local lithium-rich matrix at high temperatures, and then partially changed into grain-boundary phases after cooling (as discussed infra), similar to the Bi-rich compounds in Ref. [22]. In addition, the matrix grains slightly grew from ~4 μm to ~10 μm with increasing x, indicating that the liquid phase promoted the matrix grain growth in $Li_{2(1+x)}Mg_3ZrO_6$ ceramics. To identify the composition of the matrix and grain-boundary phase, the analysis of EDS was carried out, as shown in Table 3. The results indicate that the atomic ratio of Mg and Zr in matrix grains for both x=0 and 0.06 samples (marked as point A and C in Fig. 4) was close to 3:1, implying that the matrix grains are composed of $Li_2Mg_3ZrO_6$ phase. However, the atomic ratios of Mg and Zr in grain-boundary phases marked as point B and D greatly changed from 2:1 to 1:1 with increasing x from 0 to 0.06, indicating that the composition of the grain boundary phase was not always the same. Therefore, in combination with the XRD and SEM results, one could speculate that the grain boundary phase in current work might consist of both amorphous phase and crystalline phase $Mg_{0.13}Zr_{0.87}O_2$ including Mg, Zr, O, and Li (Li is too light to be precisely detected), in which the composition of the amorphous phase might be not constant. Although the grain-boundary phase became more with increasing x, the diffraction peak intensity of the secondary phase in the sintered samples (Fig. 2(b)) did not increase accordingly, indicating that the amorphous phase in the grain-boundary phase

Table 2
Refined structural parameters and microwave dielectric properties of $Li_{2(1+x)}Mg_3ZrO_6$ ceramics in current work and the x=0 ceramic in the literatures.

Composition	S. T.	Cubic $Li_2Mg_3ZrO_6$		Cubic ZrO_2		R_{wp} (%),R_p (%),χ^2	ε_r	$Q\times f$ (GHz)	f (GHz)	τ_f (ppm/°C)	Ref.
		V_1	m_1 (%)	V_2	m_2 (%)						
x=0	12,751,275 °C	77.565(8)	98.23(1)	133.4(1)	1.7(2)	8.98, 7.02, 1.378	12.9	206,756	9.89	−40.4	This work
x=0.02		77.532(7)	98.56(1)	134.2(2)	1.4(2)	9.07, 7.05, 1.45	13.0	195,993	9.85	−36.2	
x=0.04		77.57(1)	98.30(2)	132.8(3)	1.6(4)	10.04,7.97, 1.38	12.6	158,355	9.94	−35.5	
x=0.06		77.654(9)	98.89(1)	134.5(2)	1.1(2)	9.25, 7.13, 1.368	12.8	307,319	9.88	−37.5	
x=0.08		77.63(1)	98.51(1)	133.7(2)	1.4(3)	9.43, 7.50, 1.498	12.9	220,250	9.91	−36.9	
$Li_2Mg_3ZrO_6$	13,801,380 °C	Cubic $Li_2Mg_3ZrO_6$+Tetragonal ZrO_2				–	12.6	86000	9.3	−36	[8]
$Li_2Mg_3ZrO_6$	15201520 °C	78.02	100			11.2, 14.8, 2.354	12.2	113000	10.2	−17.1	[10]

S. T.: sintering temperature; V: unit cell volume; m: weight percent; R_{wp}, the reliability factor of weighted patterns; R_p, the reliability factor of patterns; χ^2, goodness-of-fit indicator =$(R_{wp}/R_{exp})^2$; Ref.: references.

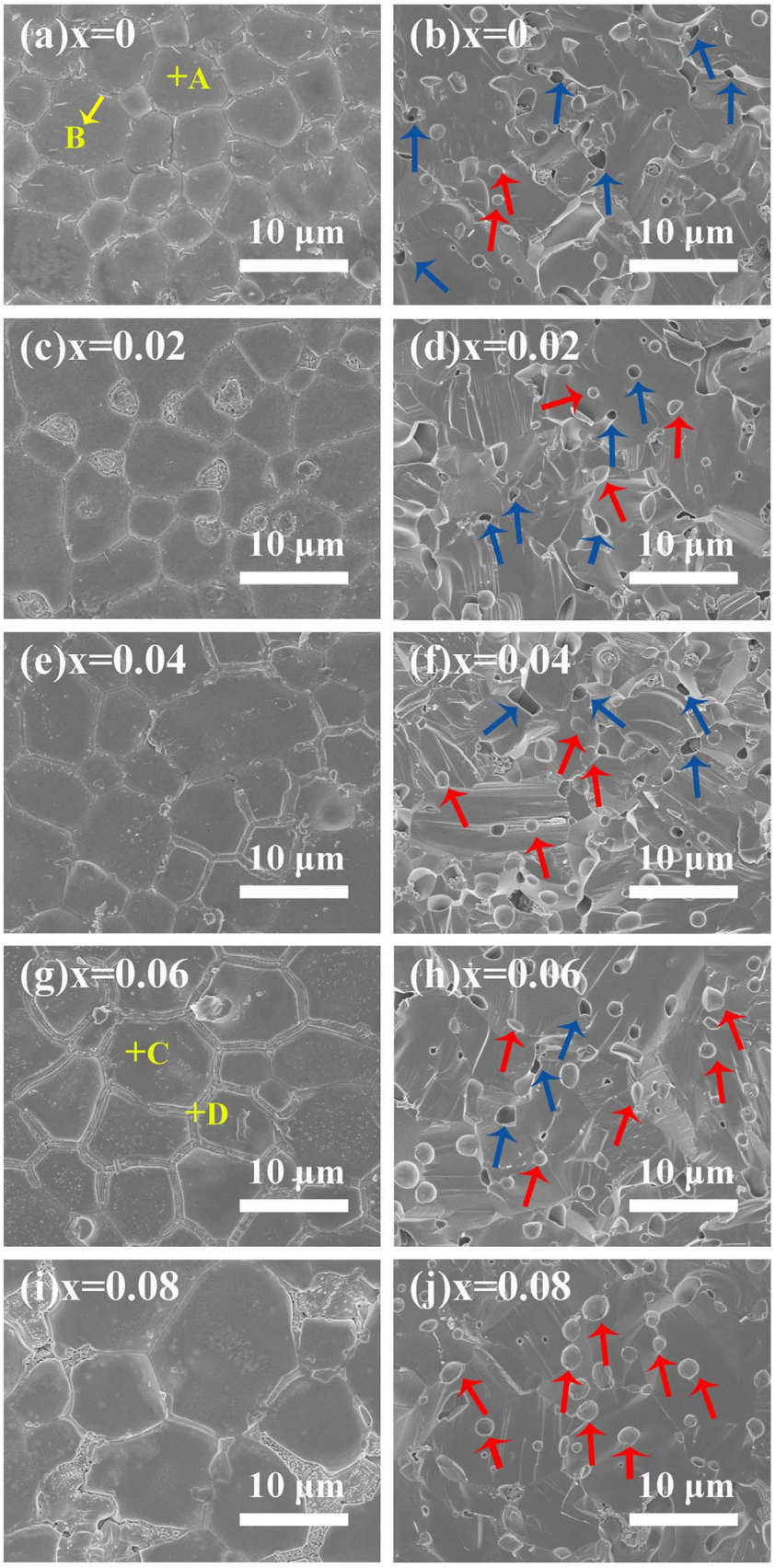

Fig. 4. SEM images of as-fired surface (a, c, e, g, i) and fractured surface (b, d, f, h, j) of $Li_{2(1+x)}Mg_3ZrO_6$ ceramics sintered at 1275 °C for 6 h. The blue and red arrows stand for the pores and grain-boundary phases, respectively. (For interpretation of the references to color in this figure legend, the reader is referred to the web version of this article.)

Table 3
EDS results of different grains marked in Fig. 4.

Elements	Atom %			
	A	B	C	D
O	44.9	38.6	50.7	57.5
Mg	39.0	41.0	35.4	23.5
Zr	16.1	20.4	13.9	19.0
Total	100.0	100.0	100.0	100.0

might be dominant. As can be seen from Fig. 4(b, d, f, h, and j), all compositions exhibited a dominant transgranular fracture mode, indicating that the fracture intensity of $Li_2Mg_3ZrO_6$ grains is so weak. In addition to the grain-boundary phase, small pores could be also found. With increasing x, the number of pores generally got less and less, which is opposite to the number of the grain-boundary phase, as indicated by blue and red arrows in Fig. 4(b, d, f, h, and j). As a result, a relatively dense microstructure was obtained as x=0.06–0.08.

The variation of bulk density and ε_r in $Li_{2(1+x)}Mg_3ZrO_6$ ceramics as a function of sintering temperature is shown in Fig. 5. As sintering temperature increased, the density of all the specimens gradually increased to their respective maximum values in the temperature range of 1275–1300 °C and then tended to decrease with further increasing sintering temperature. The variation of bulk density might be closely related to the content and distribution of the amorphous phase at the grain boundary, keeping a good consistency with the observation of microstructure in Fig. 4. Generally, ε_r mainly depends on the density, ionic polarizability, microstructure, porosity, and secondary phase [23]. As can be seen in Fig. 5, ε_r values of all compositions were ~13 in the temperature range of 1250–1325 °C owing to the combined effect of the sintering densification and the phase composition as discussed above.

Fig. 6 shows $Q\times f$ values of $Li_{2(1+x)}Mg_3ZrO_6$ ceramics sintered at different temperatures. As sintering temperature increased, $Q\times f$ values of the specimens initially increased to a maximum value approximately at 1275 °C. A further increase in sintering temperature would decrease the $Q\times f$ value probably as a result of the lithium volatilization and the density decrement. Moreover, for optimally sintered samples, the maximum $Q\times f$ value of 307,319 GHz was achieved in the x=0.06 sample. Overmany grain-boundary phases might also deteriorate the $Q\times f$ value of the x=0.08 sample, although it was relatively dense. As is well known, the $Q\times f$ value depends on the intrinsic and extrinsic factors. The former is associated with lattice anharmonicity, which is mainly affected by a particular composition and the crystal structure of the materials. The latter is related with density, impurity, secondary

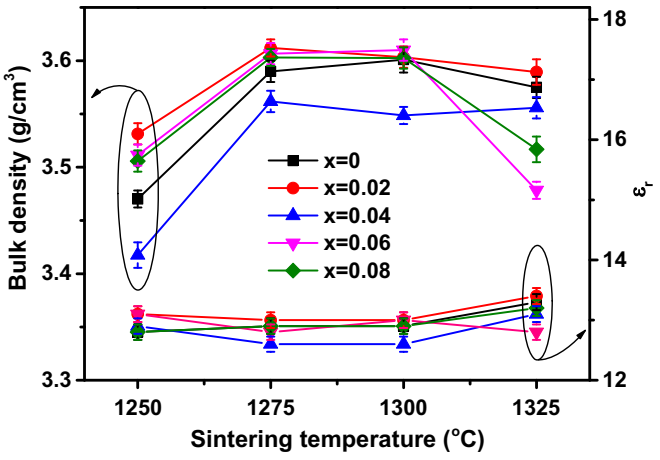

Fig. 5. Relative density and ε_r of $Li_{2(1+x)}Mg_3ZrO_6$ ceramics sintered at different temperatures.

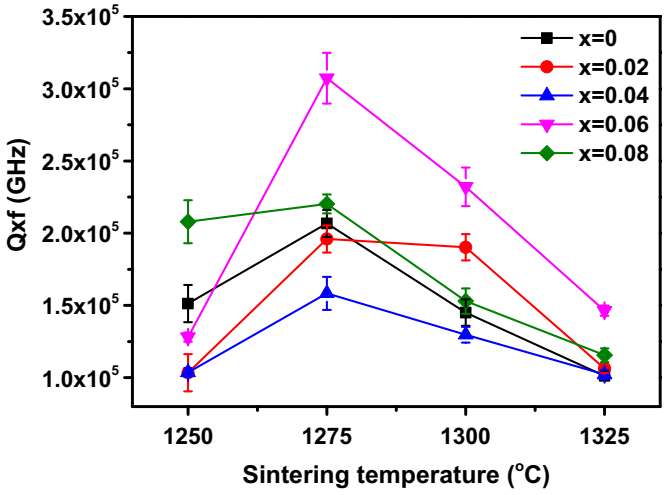

Fig. 6. $Q\times f$ of $Li_{2(1+x)}Mg_3ZrO_6$ ceramics sintered at different temperatures.

phase, grain size, microstructure, *etc.* [24] Lithium-containing materials usually have difficulties in sintering due to the lithium volatilization at high temperatures, for instance, porous Li_2TiO_3, and $Li_2Mg_3SnO_6$, *etc.* [8,10,25,26] Ding et al. [17] have reported that the addition of LiF could greatly improve the $Q\times f$ value in Li_2TiO_3 due to the modified microstructure and high density. Moreover, in our previous work [27], the substitution of $(Al_{0.5}Nb_{0.5})^{4+}$ for Ti^{4+} could significantly increase the $Q\times f$ values of Li_2TiO_3 from 55,100 to 181,800 GHz, which was also attributed to the modified microstructure. Hence, the enhancement of $Q\times f$ values in current $Li_{2(1+x)}Mg_3ZrO_6$ ceramics was primarily assigned to the denser and more uniform microstructure.

Microwave dielectric properties of $Li_{2(1+x)}Mg_3ZrO_6$ ceramics in current work and the x=0 ceramic in the literatures are compared in Table 2. It can be seen that the τ_f values in this work remained −36 ppm/°C [8], indicating no obvious effect of the excess lithium on τ_f in $Li_{2(1+x)}Mg_3ZrO_6$ ceramics. By contrast, outstanding $Q\times f$ values within the range of 150,000– 300,000 GHz and relatively low sintering temperature (1275 °C) might be of great significance in current work. This big advance in $Q\times f$ values might be attributed to the strict control of sintering atmosphere by means of the adoption of double crucibles and sacrificial powder, which could effectively suppress the lithium volatilization and promote the formation of the liquid phase, reaching a purpose of improving the sintering densification behavior and suppressing the formation of detrimental secondary phases.

4. Conclusions

$Li_{2(1+x)}Mg_3ZrO_6$ dielectric ceramics were prepared *via* a conventional solid-state synthesis method and an atmosphere-controlled sintering technique. Pure-phase $Li_2Mg_3ZrO_6$ calcined powder can be successfully achieved in this way, however, a small amount of second phases were still observed in as-sintered ceramics, which were yet obviously suppressed in the content. The lithium-rich sintering atmosphere proved to effectively suppress the lithium volatilization and help to form liquid phases at high sintering temperatures. Consequently, more homogeneous and denser microstructure, and relatively-pure phase structure (minimum secondary phases) led to the achievement of outstanding $Q\times f$ values of 150,000– 300,000 GHz. Particularly, the x=0.06 sample exhibited excellent microwave dielectric properties of ε_r=12.8, $Q\times f$=307,319 GHz (@9.88 GHz), and τ_f=−35 ppm/°C as it was sintered at 1275 °C for 6 h. This result demonstrated that $Li_2Mg_3BO_6$ (B=Ti, Zr, Sn) might be a family of desirable microwave dielectric ceramics only if issues concerning the lithium loss, densification and phase purity could be well solved.

Acknowledgments

This work was financially supported by the National Natural Science Foundation of China (Grant no. 51272060).

References

[1] M.T. Sebastian, Dielectric Materials for Wireless Communications, Elsevier Publishers, Oxford, U.K, 2008.
[2] S.B. Narang, S. Bahel, Low loss dielectric ceramics for microwave applications: a review, J. Ceram. Process Res. 11 (2010) 316–321.
[3] M.T. Sebastian, H. Jantunen, Low loss dielectric materials for LTCC applications: a review, Int. Mater. Rev. 53 (2008) 57–90.
[4] H.F. Zhou, X.B. Liu, X.L. Chen, L. Fang, Y.L. Wang, $ZnLi_{2/3}Ti_{4/3}O_4$: a new low spinel microwave dielectric ceramic, J. Eur. Ceram. Soc. 32 (2012) 261–265.
[5] C.L. Huang, J.J. Wang, C.Y. Huang, Microwave dielectric properties of sintered alumina using nano-scaled powders of alpha alumina and TiO_2, J. Am. Ceram. Soc. 90 (2007) 1487–1493.
[6] T. Tsunooka, M. Androu, Y. Higashida, H. Sugiura, H. Ohsato, Effects of TiO_2 on sinterability and dielectric properties of high-*Q* forsterite ceramics, J. Eur. Ceram. Soc. 23 (2003) 2573–2578.
[7] Y. Guo, H. Ohsato, K.I. Kakimoto, Characterization and dielectric behavior of willemite and TiO_2-doped willemite ceramics at millimeter-wave frequency, J. Eur. Ceram. Soc. 26 (2006) 1827–1830.
[8] Z. Fu, P. Liu, J. Ma, X. Zhao, H. Zhang, Novel series of ultra-low loss microwave dielectric ceramics: $Li_2Mg_3BO_6$ (B=Ti, Sn, Zr), J. Eur. Ceram. Soc. 36 (2016) 625–629.
[9] Z. Fu, P. Liu, J. Ma, X. Chen, H. Zhang, New high *Q* low-fired $Li_2Mg_3TiO_6$ microwave dielectric ceramics with rock salt structure, Mater. Lett. 164 (2016) 436–439.
[10] H. Wu, E.S. Kim, Correlations between crystal structure and dielectric properties of high-*Q* materials in rock-salt structure Li_2O–MgO–BO_2 (B = Ti, Sn, Zr) systems at microwave frequency, Rsc Adv. 6 (2016) 47443–47453.
[11] P. Zhang, H. Xie, Y. Zhao, M. Xiao, Microwave dielectric properties of low loss $Li_2(Mg_{0.95}A_{0.05})_3TiO_6$ (A=Ca^{2+}, Ni^{2+}, Zn^{2+}, Mn^{2+}) ceramics system, J. Alloy. Compd. 689 (2016) 246–249.
[12] Z.Fang, B.Tang, F.Si, S.Zhang, Temperature stable and high-Q microwave dielectric ceramics in the $Li_2Mg_{3-x}Ca_xTiO_6$ system (x=0.00–0.18), Ceram. Int. ⟨http://dx.doi.org/10.1016/j.ceramint.2016.08.055⟩.
[13] Z. Fu, P. Liu, J. Ma, B. Guo, X. Chen, H. Zhang, Microwave dielectric properties of low-fired Li_2SnO_3 ceramics co-doped with MgO–LiF, Mater. Res. Bull. 77 (2016) 78–83.
[14] J. Zhang, R.Z. Zuo, Synthesis and microwave dielectric properties of $Li_2Mg_2(WO_4)_3$ ceramics, Mater. Lett. 158 (2015) 92–94.
[15] J. Zhang, R.Z. Zuo, Y. Wang, S.S. Qi, Phase evolution and microwave dielectric properties of $Li_4Ti_{5(1+x)}O_{12}$ ceramics, Mater. Lett. 164 (2016) 353–355.
[16] J.J. Bian, Y.F. Dong, Sintering behavior, microstructure and microwave dielectric properties of $Li_{2+x}TiO_3$ ($0 \le x \le 0.2$), Mater. Sci. Eng. B 176 (2011) 147–151.
[17] Y. Ding, J.J. Bian, Structural evolution, sintering behavior and microwave dielectric properties of $(1-x)Li_2TiO_3+xLiF$ ceramics, Mater. Res. Bull. 48 (2013) 2776–2781.
[18] M. Castellanos, A.R. West, W.B. Reid, Dilithium magnesium zirconium tetraoxide with an α-$LiFeO_2$ structure, Acta Crystallogr. C 41 (1985) 1707–1709.
[19] A.C. Larson, R.B. Von Dreele, General Structural Analysis System (GSAS), Report LAUR 86-748, Los Alamos National Laboratory, Los Alamos, NM, 2000.
[20] B.H. Toby, EXPGUI, a Graphical User Interface for GSAS, J. Appl. Crystallogr. 34 (2001) 210–213.
[21] B.W. Hakki, P.D. Coleman, A dielectric resonantor method of measuring inductive capacities in the millimeter range, IEEE Trans. Microw. Theory Technol. 8 (1960) 402–410.
[22] X.H. Ma, S.H. Kweon, S. Nahm, C.Y. Kang, S.J. Yoon, Y.S. Kim, W.S. Yoon, Microstructural and microwave dielectric properties of $Bi_{12}GeO_{20}$ and Bi_2O_3-deficient $Bi_{12}GeO_{20}$ ceramics, J. Am. Ceram. Soc. 99 (2016) 2361–2367.
[23] Q.W. Liao, L.X. Li, X. Ren, X. Ding, New low-loss microwave dielectric material $ZnTiNbTaO_8$, J. Am. Ceram. Soc. 94 (2011) 3237–3240.
[24] S.J. Penn, N.M. Alford, A. Templeton, X. Wang, M. Xu, M. Reece, K. Schrapel, Effect of porosity and grain size on the microwave dielectric properties of sintered alumina, J. Am. Ceram. Soc. 80 (1997) 1885–1888.
[25] J.J. Bian, Y.F. Dong, New high *Q* microwave dielectric ceramics with rock salt structures: $(1-x)li_2TiO_3+xMgO$ system ($0 \le x \le 0.5$), J. Eur. Ceram. Soc. 30 (2010) 325–330.
[26] C.L. Huang, Y.W. Tseng, J.Y. Chen, High-*Q* dielectrics using ZnO-modified Li_2TiO_3 ceramics for microwave applications, J. Eur. Ceram. Soc. 32 (2012) 3287–3295.
[27] T.W. Zhang, R.Z. Zuo, J. Zhang, Structure, microwave dielectric properties and low-temperature sintering of acceptor/donor codoped $Li_2Ti_{1-x}(Al_{0.5}Nb_{0.5})_xO_3$ ceramics, J. Am. Ceram. Soc. 99 (2016) 825–832.